Research Article

Received: 5 June 2019 Revised: 22 July 2019 Accepted article published: 2 August 2019 Published online in Wiley Online Library: 22 August 2019

(wileyonlinelibrary.com) DOI 10.1002/pi.5896

Endocytosis behaviours of nanoparticles with helically decorated ligands

Zhou Guan, Liquan Wang,* Jiaping Lin* and Jiaxiao Xue

Abstract

In this work, the receptor-mediated endocytosis of nanoparticles with helically decorated ligands was investigated by performing coarse-grained molecular dynamics simulations. The results showed that a helical distribution of ligands can generate a unique spinning stage during endocytosis in which the nanoparticle is internalized with precession. This precession behaviour is primarily caused by a lateral torque acting on the nanoparticle. Compared with nanoparticles that present uniformly distributed ligands, nanoparticles with helically decorated ligands present an enhanced endocytosis capacity. Additionally, a longer spin duration and larger precessional angle were obtained by decreasing the helical period of the ligands. Increasing the aspect ratio of the nanoparticles strengthens their capacity to take the spinning endocytosis pathway. The present study not only reveals the mechanism underlying a new endocytosis pathway of nanoparticles with helically structured surfaces but also provides valuable theoretical information for the design of novel drug delivery systems that primarily occur via cellular uptake.

Supporting information may be found in the online version of this article.

Keywords: biopolymers; nanoparticle with ligands; cellular internalization; theoretical simulation

INTRODUCTION

Endocytosis is the universal process through which cells internalize objects, such as proteins, molecules, viruses and nanoparticles.[1–4] Among the various endocytosis pathways (e.g. receptor-mediated endocytosis, caveolae-mediated endocytosis, pinocytosis and phagocytosis),[5–8] receptor-mediated endocytosis has received considerable attention recently because it is the most likely pathway for the entry of drug delivery vehicles (e.g. nanoparticles, block copolymer micelles, vesicles and dendrimers) into lesion cells.[3,9–12] By loading drugs inside those delivery systems, drug accumulation occurs in cells and reduced cytotoxicity can be achieved. In receptor-mediated endocytosis, particles with biocompatible surfaces bind strongly to receptors (e.g. cholesterol and membrane protein) on the membrane, which leads to efficient engulfment and internalization by cells. By decorating the particle surface with ligands (e.g. electrolytes, peptides and proteins),[13–15] enhanced cellular uptake performance and even targeted delivery can be achieved. Therefore, understanding the effect of ligands on the behaviour of receptor-mediated endocytosis is significant for academic studies and biomedical applications.

Recently, considerable research effort has been focused on evaluating ligands that decorate the substrates of nanoparticles and examining their endocytosis behaviours. In experimental investigations, various biocompatibility ligands were adopted, and new techniques for decorating those ligands on the surface of delivery vehicles were explored.[16–19] For example, Sawant *et al.* studied the cellular uptake capacity of poly(ethylene glycol)-phosphatidylethanolamine micelles,[16] and they found that, by modifying transferrin at the hydrophilic end of the polymers, the cellular internalization capacities of these micelles can be effectively enhanced because of the strong binding between transferrin and transferrin receptors during endocytosis. In addition to the experiments, theoretical studies have focused on the effects of ligands on endocytosis behaviours, such as the ligand–receptor binding strength and the surface density of ligands.[20–23] For example, Li *et al.* used dissipative particle dynamics (DPD) simulations to study the endocytosis of nanoparticles grafted with polyethylene glycol (PEG) polymers,[20] and they found that increasing the surface density of ligands can benefit endocytosis. In addition to the DPD simulation method, coarse-grained molecular dynamics (CGMD) simulation approaches have been developed and applied to investigate the receptor-mediated endocytosis behaviour of nanoparticles.[24–28] The various molecular potentials involved in CGMD methods are physically suitable for simulating biological systems, such as cell membranes. For example, the solvent-free model proposed by Cooke *et al.*, which maintains the principal properties of the cell membrane (e.g. bending modulus, surface tension and diffusion constant),[26] has been adopted to simulate the endocytosis of nanoparticles. With this method, a deeper understanding of the mechanisms of endocytosis was gained. For example, a critical radius value was observed for the completion of endocytosis by spherical nanoparticles.[28]

Recently, the topological distribution of ligands on the particle surface was found to influence the cellular uptake

* *Correspondence to: L Wang or J Lin, Shanghai Key Laboratory of Advanced Polymeric Materials, Key Laboratory for Ultrafine Materials of the Ministry of Education, School of Materials Science and Engineering, East China University of Science and Technology, Shanghai 200237, China. E-mail: lq_wang@ecust.edu.cn (Wang); jlin@ecust.edu.cn (Lin)*

Shanghai Key Laboratory of Advanced Polymeric Materials, Key Laboratory for Ultrafine Materials of the Ministry of Education, School of Materials Science and Engineering, East China University of Science and Technology, Shanghai, China

performance.[29–32] For example, Schubertová *et al.* found that nanoparticles with homogeneously distributed ligands exhibited a shorter endocytosis duration.[29] Studies published on receptor-mediated endocytosis have generally focused on the distribution of ligands in the form of separate patches (i.e. ligands form several domains on the substrates).[23,29] Other possible topological distributions have not been addressed. Reports have shown that ligands with a stripe-like distribution may improve the cell-penetrating capacities of small nanoparticles (at approximately 4 nm in diameter, the cellular uptake pathway occurs via direct penetration not endocytosis).[30,31] Inspired by this evidence, large nanoparticles (larger than 10 nm in diameter) decorated with ligands in a stripe-like distribution pattern may exhibit a unique endocytosis pathway or performance. However, relevant investigations addressing this issue have not been conducted; thus, the endocytosis of large nanoparticles with stripe-patterned ligands remains unknown.

Viruses are among the most ubiquitous nanoparticles in nature and can provide insights into the facile topological distributions of ligands on particle surfaces.[29,33–36] Among these surface structures, helices are observed in several families of virus particles (e.g. tobacco mosaic virus and Poxviridae). This surface topology has been successfully imitated in the substrates of laboratory-prepared particles.[37–40] For example, Cai *et al.* recently discovered that poly(γ-benzyl-L-glutamate)-*b*-poly(ethylene glycol) (PBLG-*b*-PEG) rod–coil block copolymers and rigid PBLG homopolymers were able to co-assemble into virus-like super-helical rods.[37] In these structures, the homopolymers serve as a cylindrical template on which the block copolymers self-assemble into helix-like nanostructures. The distal methoxy group of PEG blocks, which forms the corona of the helix bundle, can be regarded as a proper ligand because it can bind to receptors on the plasma membrane.[41,42] These polymeric aggregates can be modelled as nanoparticles with helically decorated ligands, which have been proved to be capable in cellular internalizations by means of endocytosis.[43] However, the detailed endocytosis pathways of these nanoparticles and the explicit role played by the uniquely distributed ligands have not been well addressed. Because experimental approaches cannot easily obtain molecular-level insights into nanoparticle–membrane interaction procedures (e.g. how nanoparticles enter cells), the CGMD simulation represents a powerful tool that can be used to address the above challenges.

In the present study, we performed CGMD simulations to investigate the receptor-mediated endocytosis of nanoparticles with helically decorated ligands. First, we studied the endocytosis kinetics. Compared with traditional nanoparticles that present uniformly packed ligands, enhanced endocytosis capacity was observed for nanoparticles with helically decorated ligands. The mechanisms underlying this enhanced endocytosis capacity were analysed. Then, we examined the effects of the initial contact angle, the ligand helix period and the nanoparticle aspect ratio on endocytosis behaviour. The present study provides important insights on the endocytosis of nanoparticles decorated with helical ligands, and our findings may provide valuable theoretical information for the design of nanoparticles used in biological environments, such as drug delivery systems.

SIMULATION METHOD

Herein, we constructed a system that contains a ligand-decorated nanoparticle and a plasma membrane. The models are illustrated

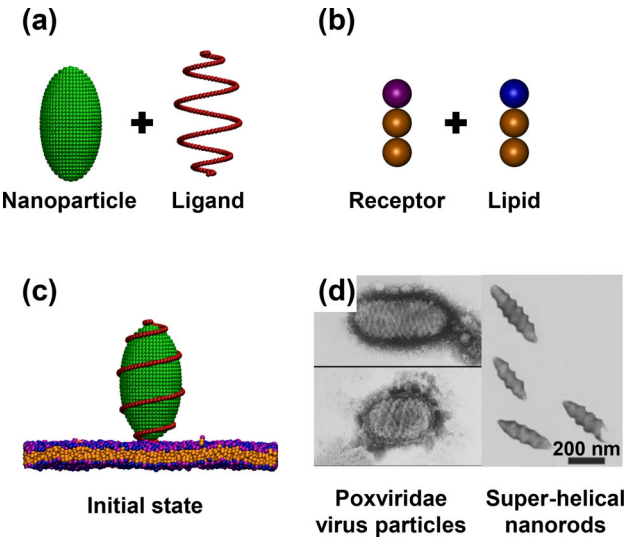

Figure 1. Model of the simulation. (a) Ellipsoidal nanoparticle and helical ligand; (b) phospholipid and receptor; (c) initial status of the system. The nanoparticle with helical ligands can serve as a model for (d) the Poxviridae virus particle and super-helical nanoparticles prepared in our previous work.[39] The image of the virus particles in (d) is reproduced from Wikipedia under the entry 'Parapoxvirus'.[44] The super-helical nanoparticles in (d) are reproduced with permission of ref. [39], Copyright 2011, Royal Society of Chemistry.

in Fig. 1. Figure 1(a) shows the model of the nanoparticle and ligand. The coarse-grained nanoparticle model (shown in green) is presented as a hollow ellipsoid substrate formed by beads. Helically distributed ligands (shown in red) are compactly decorated on the substrate of the particle. The nanoparticle and ligand are fixed as a rigid body in the simulations. The model of the bilayer plasma membrane formed by phospholipids is shown in Fig. 1(b). According to the solvent-free model proposed by Cooke *et al.*,[26] the coarse-grained phospholipid model consists of three beads connected by harmonic bonds. The head lipid bead is hydrophilic and shown in purple. The two tail beads are hydrophobic and are shown in orange. A specific amount of lipids in the membrane are receptors, which have head beads shown in blue and strongly bind to the ligands of nanoparticles. The ligand-decorated nanoparticle is in intense contact with the membrane, and it can serve as a model of the virus particle of Poxviridae[44] and the super-helical rod-like nanoparticles prepared in our previous study,[39] as shown in Figs 1(c), 1(d).

Although the complexity of cell membranes is not precisely represented, this coarse-gained model successfully maintains the essential features of the cell membrane, such as the bending module, fluidity and the binding between ligands and receptors.[26] Using this model, results that agree with experimental observations were gained in existing theoretical simulation work.[25,28] We believe that this simulation method is capable of revealing the cellular uptake behaviours of nanoparticles.

The molecular potentials and parameters were all set according to those used in published work.[25,26,28,29] For lipids, a finite extensible nonlinear elastic potential was adopted for defining the bonds linking two neighbouring beads:

$$U_{\text{bond}}(r) = -\frac{1}{2}k_b r_b^2 \ln\left[1-\left(\frac{r}{r_b}\right)^2\right] \quad (1)$$

In this equation, the strength k_b is $30\varepsilon_0/\sigma^2$ and the maximum extent r_b of the bond is 1.5σ. Here, ε_0 and σ denote the energy and

length unit, respectively. Additionally, a harmonic spring potential is applied between the head and second tail beads to maintain the straightened shape of the lipids:

$$U_{\text{angle}}(r) = \frac{1}{2}k_a(r - r_a)^2 \quad (2)$$

In this equation, the strength $k_a = 10\varepsilon_0/\sigma^2$ and the equilibrium bond distance $r_a = 4\sigma$. The value of r_a is set to be larger than $2r_b$ (3σ) so that the stiffness of lipids in the simulations can be maintained. This value was also adopted in some reported simulation work.[24–26]

In this model, the potential energy among all the beads is represented as follows:

$$U_{\text{all}}(r) = \begin{cases} 4\varepsilon_0[(\lambda\sigma/r)^{12} - (\lambda\sigma/r)^6] & r < r_{\text{cut}} \\ -\varepsilon_{\text{atr}}\cos^2[\pi(r - r_{\text{cut}})/2r_{\text{atr}}] & r_{\text{cut}} \le r \le r_{\text{cut}} + r_{\text{atr}} \\ 0 & r > r_{\text{cut}} + r_{\text{atr}} \end{cases} \quad (3)$$

The top part of the function is the Lennard-Jones potential. In addition, ε_0 is the interaction strength and is set as the unit energy, σ is the length unit and $r_{\text{cut}} = 2^{1/6}\lambda_{ij}\sigma$. The values of λ_{HH} and λ_{HT} were both set to 0.95, and the subscripts H and T denote the head/ligand and tail beads of the phospholipids, respectively. The values of λ_{ij} for other beads were all set to 1. The middle part of the function represents the attraction between all the tail beads of the lipids as well as the binding between ligands and receptors. For the tail beads, $\varepsilon_{\text{atr}} = \varepsilon_0$ and $r_{\text{atr}} = 2.53\sigma$, which should represent the optimal values for obtaining a plasma membrane. For a pair of ligand and receptor, ε_{atr} was set to $4\varepsilon_0$ unless otherwise specified. Moreover, r_{atr} was set to 1.45σ, which was used as a proper value in the simulation work by Vácha *et al.*[28]

During the endocytosis, the nanoparticles are continuously engulfed by lipids. The membrane has to keep a constant lateral tension to provide enough lipids for this engulfment. To simulate the endocytosis behaviour of nanoparticles, we adopted constant lateral tension conditions in the simulations. A modified Berendsen barostat was used to maintain the desired lateral tension. According to the current membrane lateral tension, the simulation box and bead coordinates were rescaled in the dimensions parallel to the membrane (i.e. *x*/*y* dimensions in our simulations). The scaling factor $\lambda_{x/y}$ is determined as follows:[45]

$$\lambda_{x/y} = 1 + \frac{[\Gamma_0 - \Gamma(t)]\mathrm{d}t}{T_{\text{rel}}K} \quad (4)$$

where dt is the time step, T_{rel} is the relaxation time, K is the compression modulus, and Γ_0 and $\Gamma(t)$ denote the desired tension and the current membrane lateral tension, respectively:

$$\Gamma(t) = -\frac{P_{xx}(t) + P_{yy}(t)}{2} \quad (5)$$

In our simulation system, T_{rel} and K were set to 100 and 0.001, respectively. All the simulations were run under conditions with zero membrane tension (i.e. $\Gamma_0 = 0$). In addition, the simulations were performed under a constant temperature. A Langevin thermostat, which was developed by Schneider and colleagues, was adopted. The beads were coupled to a heat bath. The equation of motion is written as follows:[46]

$$m_i\frac{\mathrm{d}\boldsymbol{v}_i}{\mathrm{d}t} = \boldsymbol{F}_i - \zeta\boldsymbol{v}_i + \boldsymbol{W}_i(t) \quad (6)$$

where m_i and $\boldsymbol{v}_i$ are the mass and velocity of the ith bead, respectively; $\boldsymbol{F}_i$ is the force acting on the ith bead, calculated by the potential energies consisting of $U_{\text{bond}}(r)$, $U_{\text{angle}}(r)$ and $U_{\text{all}}(r)$; and ζ is a friction constant. In Langevin dynamics, the effects of solvent molecules are implicitly treated by the noise term $\boldsymbol{W}_i(t)$, which can be calculated according to the fluctuation–dissipation relation:[47,48]

$$\langle \boldsymbol{W}_i(t) \cdot \boldsymbol{W}_j(t') \rangle = 6k_{\text{B}}T\zeta\delta_{ij}(t - t') \quad (7)$$

where k_{B} is the Boltzmann constant. Under the $N\Sigma T$ ensemble (N, Σ and T denote the number of beads, the membrane lateral tension and the system temperature, respectively), all simulations are conducted in a cubic cell with an initial size of $70 \times 70 \times 70$ σ^3. A membrane formed by 4400 lipids is set in the middle of the box, and the surface is perpendicular to the z axis. Fifty per cent of the lipids are receptors. The semi-lengths of the long (r_a) and short (r_b) axes of the nanoparticle are set as 15σ and 8σ, respectively. The number of beads forming ligands was fixed at 147. The CGMD simulations were run for at least 5×10^6dt, where the time step dt was set to 0.01τ. The length unit σ and time unit τ were converted to 1 nm and 0.01 μs, respectively, according to the diffusion constant of the membrane (Supporting Information, Section S1).

RESULTS

Spin behaviour of nanoparticles with helically decorated ligands

First, the receptor-mediated endocytosis of nanoparticles with helically decorated ligands was studied. Snapshots of the endocytosis process are illustrated in Fig. 2. Generally, endocytosis follows a traditional process.[28] After the initial contact with the membrane, the nanoparticle is gradually engulfed by the membrane as shown in Figs 2(a)–2(d). Subsequently, the nanoparticle is entirely engulfed by the membrane, and a vesicle is formed. The vesicle is connected to the membrane via a lipid 'neck' as shown in Fig. 2(e). After the neck breaks, the vesicle is detached from the membrane as shown in Fig. 2(f), and the receptor-mediated endocytosis process is completed. After carefully examining the endocytosis process of the nanoparticle, we found that the nanoparticle spins while it is endocytosed. The spin behaviour includes precession and rotation. The schematic illustration of the precession during endocytosis is shown in Fig. 2(g).

The unique spin phenomenon observed in the present study is rarely reported in studies of the endocytosis of nanoparticles. To reveal the spin behaviours of the nanoparticle, we studied the spinning trajectories during endocytosis. The results are presented in Fig. 3. Figure 3(a) shows the profiles of angles θ, φ (corresponding to precession) and γ (corresponding to rotation) and the wrapping percentage of the nanoparticle (η) as a function of time. Figure 3(b) illustrates the definitions of the angles θ, φ and γ. Regarding the rotation, the nanoparticle spins around its own major axis as shown in Fig. 3(b), where γ denotes the rotated angle. For the precession aspect, the major axis of the nanoparticle reorients and spins around another axis vertical to the membrane (i.e. the z axis in the simulation box) as shown in Fig. 3(b). θ denotes the angle between the major axis of the nanoparticle and its precession axis, and the precession angle is denoted by φ. The value of the angle φ is calculated by the projection of the nanoparticle main axis on the membrane plane (x/y plane), oscillating between 0 and π. As shown in Fig. 3(a), endocytosis is completed at 360 μs

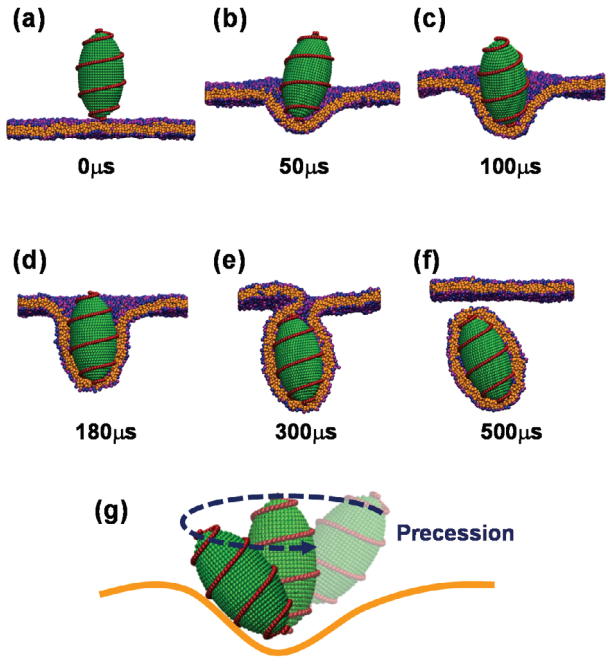

Figure 2. Snapshots during endocytosis: (a) initial contact between the nanoparticle and the membrane; (b)–(d) engulfing the nanoparticle; (e) the lipid-formed vesicle is connected to the membrane with a 'neck'; (f) after the neck is broken, the vesicle detaches from the membrane. (g) Schematic illustration of the precession behaviour during endocytosis.

according to the profile of η (i.e. η reaches 100% at 360 μs). Prior to 360 μs, the value of η gradually increases, which indicates that the engulfment rate of the nanoparticle is nearly constant. Regarding rotation, the γ angle evolves from 0 to $\pi/2$ before 150 μs; subsequently, the angle is mostly unchanged. This phenomenon suggests that the nanoparticle rotates around its own major axis at an angle of approximately $\pi/2$ before 150 μs and stops rotating after that. That the rotation is stopped at 150 μs may be because there is insufficient free space as more than half of the nanoparticle surface is engulfed by lipids after 150 μs. For the precession aspect, the θ angle is close to but larger than 0. The profile of the φ angle presents a sine/cosine wave before 300 μs, and the sine/cosine curve has approximately two and a half periods. After 300 μs, the φ angle slightly fluctuates around 0. The evolution of the θ and φ angles before 300 μs indicates that the nanoparticle precesses for two and a half periods with its major axis nearly vertical to the membrane. According to the spin behaviour of the nanoparticle, the endocytosis procedure can be divided into three stages: spinning stage (both rotation and precession can be observed), spinning-free stage (i.e. the nanoparticle stops spinning but has not been completely endocytosed) and the end of endocytosis stage (i.e. endocytosis is complete). In Fig. 3(a), the three stages are denoted by the letters S, SF and E. Movies showing the endocytosis procedure can be found in the Videos S1 and S2.

A comparison of the rotation and precession behaviours showed that the precession is much stronger (the particle precesses by two and a half periods) than the rotation (the particle rotates at a small angle). In addition, a control study of the endocytosis of a nanoparticle uniformly decorated with ligands was performed, and the results showed the rotation phenomenon in the endocytosis procedure. However, precession does not occur in this endocytosis process. Details of the control study can be found in the Supporting Information, Section S2. Therefore, in the study on the spinning behaviour of nanoparticles, we considered only the precession behaviour.

In addition to the spinning trajectories, we further studied the mechanisms of precession by examining the precessional torque ($\boldsymbol{\tau}_{\text{pre}}$) on the nanoparticle. The evolution of the torque during endocytosis is presented in Fig. 4. Figures 4(b) and 4(c) represent the schematics of the torque acting on the nanoparticle. Herein, $\boldsymbol{\tau}_{\text{pre}}$ is the sum of all torque for all beads that compose the nanoparticle and ligands:

$$\boldsymbol{\tau}_{\text{pre}} = \sum_{n=1}^{n=N} \boldsymbol{r}_n \times \boldsymbol{F}_n \tag{8}$$

where $\boldsymbol{r}_n$ and $\boldsymbol{F}_n$ denote the lever arm relative to the precession pivot and the force acting on the bead n, respectively, as shown in Figs 4(b) and 4(c); and N is the total number of beads that compose the nanoparticle and ligands.

Figure 4(a) shows the profiles of the torque in three orthogonal directions (τ_x, τ_y and τ_z) and indicates that τ_x and τ_y present cosine and sine waves, respectively, before 300 μs and their curves have a phase difference of approximately a quarter period. Therefore, the torque acting on the nanoparticle in the xy plane is almost unchanged before 300 μs. τ_z fluctuates around 0 all the time. The torque profiles before 300 μs indicate that the forces acting on the nanoparticle drive the particle precession around an axis vertical to the membrane. After 300 μs, τ_x and τ_y are both gradually reduced to 0 and fluctuate around 0, which means that precession stops. Compared with the precession trajectory in Fig. 3, the torques (τ_x and τ_y) and φ angle have the same periods and sine/cosine wave duration. This synchronization also shows that the torques in the x and y directions are responsible for the precession.

In our simulations, we also discovered that the precession behaviours depend on the ligand–receptor binding strength. We performed simulations by increasing the ligand–receptor binding strength (denoted by ε_{atr} in Eqn (3)). A large ε_{atr} could represent a more bio-active ligand decorated on the nanoparticle surface, such as transferrin and low-density lipoprotein. In addition to a faster endocytosis, we also observed that the proportion of the precession duration to the entire endocytosis duration decreased (i.e. $T_{\text{spinning}}/T_{\text{endocytosis}}$ became smaller, where T denotes time) with increasing ε_{atr}.

Endocytosis capacity of the nanoparticles with helically decorated ligands

The simulations indicate that nanoparticles with helically decorated ligands can spontaneously spin during endocytosis. This endocytosis pathway may contribute to a unique cellular uptake performance. We performed endocytosis simulations for two types of nanoparticles to provide deep insights into the cellular uptake capacity contributed by this unique endocytosis pathway. One type of nanoparticle is helically decorated with ligands and the other has uniformly distributed ligands (denoted by H and U, respectively). These two types of nanoparticles have ligands with the same size ($r_a = 15\sigma$ and $r_b = 8\sigma$) and surface density ($\xi_L = 0.08/\sigma^2$). A smaller receptor–ligand binding strength ε_{atr} of $3\varepsilon_0$ is adopted. By analysing the simulated results, the endocytosis capacities of these two types of nanoparticles were compared.

The snapshots during endocytosis of these two nanoparticles under a binding strength of $\varepsilon_{\text{atr}} = 3\varepsilon_0$ are presented in Fig. 5. The

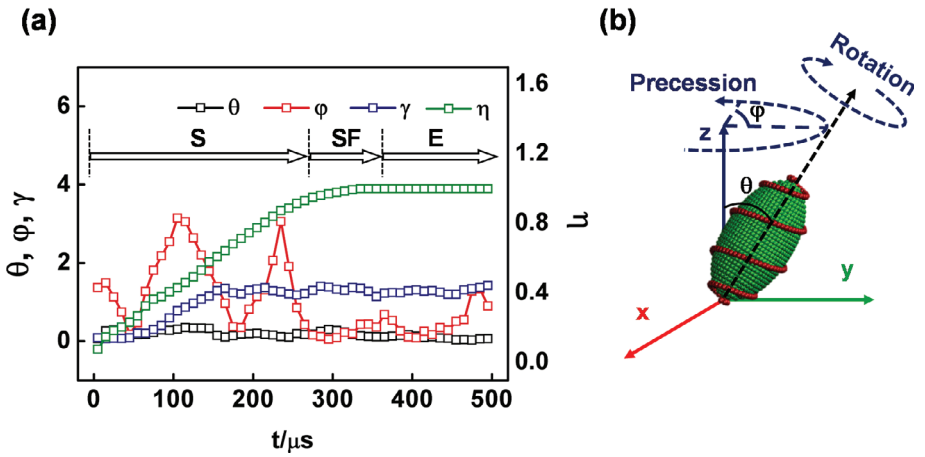

Figure 3. (a) Spinning trajectory (denoted by the evolution of θ, φ and γ) and wrapping ratio (η) during endocytosis of a particle with helix period $P = 5$ and initial contact angle $\theta_0 = 0$. (b) Schematic illustrations of precession and rotation denoted by angles θ, φ and γ. S, SF and E in (a) denote the spinning, spinning-free and end of endocytosis stages, respectively.

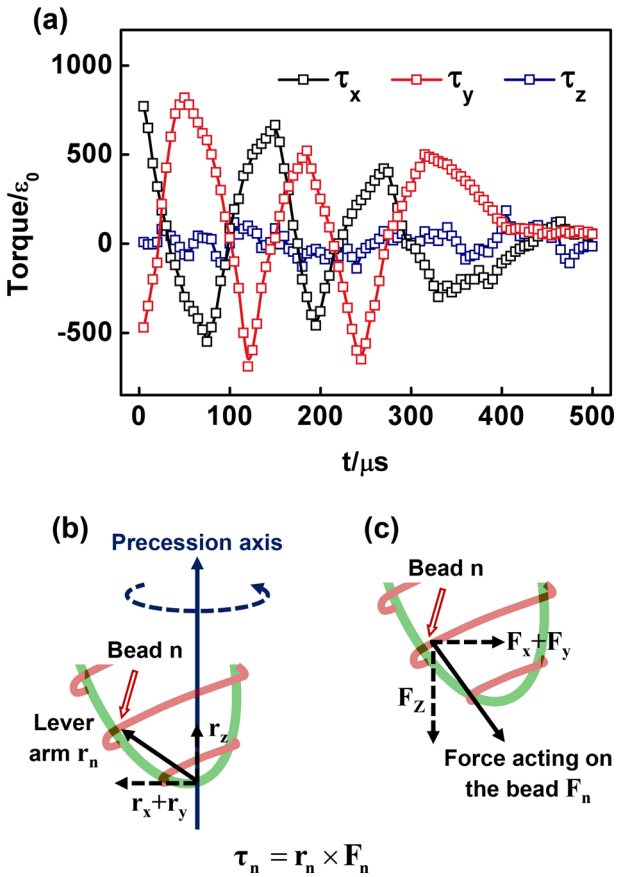

Figure 4. (a) Torque on the nanoparticle relative to its precession pivot. (b), (c) Schematic illustrations of the lever arm ($\boldsymbol{r}_n$) and the force acting on the nth bead ($\boldsymbol{F}_n$). The three orthogonal components of $\boldsymbol{r}_n$ and $\boldsymbol{F}_n$, which are denoted by $\boldsymbol{r}_x$, $\boldsymbol{r}_y$, $\boldsymbol{r}_z$ and $\boldsymbol{F}_x$, $\boldsymbol{F}_y$, $\boldsymbol{F}_z$, are presented in (b) and (c), respectively.

endocytosis procedures of nanoparticles H and U with an initial contact angle $\theta_0 = 0$ (vertical contact) are shown in Figs 5(a) and 5(b), respectively. Nanoparticle H is shown to endocytose within 600 μs, and the orientation angle during endocytosis is relatively small (i.e. a preference for tip-oriented endocytosis), as shown in Fig. 5(a). However, nanoparticle U prefers a larger orientation angle (i.e. a preference for side orientation) while being endocytosed and cannot be totally engulfed and endocytosed, as shown in Fig. 5(b). Although the nanoparticle is intensely attached to the membrane, a vesicle is not formed and endocytosis cannot be accomplished, even when the simulation is performed for 800 μs. A similar phenomenon can be observed when the two nanoparticles endocytose with an initial contact angle of $\theta_0 = \pi/2$ (horizontal contact). As shown in Fig. 5(c), nanoparticle H exhibits a side-oriented entry and can be endocytosed within 350 μs, and nanoparticle U remains side oriented before 200 μs and becomes tip oriented after 600 μs. The endocytosis duration for the nanoparticle in Fig. 5(c) is shorter than that in Fig. 5(a) as a result of closer nanoparticle–membrane initial distance. However, endocytosis is not completed even after 800 μs for nanoparticle U. Figure 5(d) shows that the vesicle formed by lipids cannot be completely formed, which results in endocytosis failure. Moreover, the failed endocytosis of nanoparticle U can be observed only under a smaller receptor–ligand binding strength ($\varepsilon_{atr} = 3\varepsilon_0$). When the binding strength is strengthened (e.g. $\varepsilon_{atr} > 3\varepsilon_0$), nanoparticle U can accomplish endocytosis. The duration of endocytosis of nanoparticle U is longer than that of nanoparticle H.

The simulation results indicate better endocytosis for nanoparticle H than for U. Herein, we attempted to further reveal the mechanisms underlying this phenomenon. According to the Helfrich formula, during endocytosis the particle should overcome the bending energy of the plasma membrane:[49]

$$E_B = \int_\eta A\left[\frac{\kappa}{2}(C_1 + C_2 - C_0)^2 + \frac{\kappa_G}{2}(C_1C_2)^2\right] d\eta \qquad (9)$$

where κ and κ_G are the bending moduli of the mean and Gaussian curvature of the membrane, respectively; A is the area of the membrane that has already engulfed the particle; η is the wrapping ratio of the nanoparticle ($0 \le \eta \le 1$); C_1 and C_2 are the local principal curvatures; and C_0 denotes the spontaneous curvature of the membrane. For membranes simulated under zero surface tension, $C_0 = 0$.

Using the Helfrich formula, we calculated the evolutionary membrane bending energies during the endocytosis of nanoparticles H and U initiated from contact angles $\theta_0 = 0$ and $\pi/2$. The receptor–ligand binding strength ε_{atr} was set to $4\varepsilon_0$. In this case, the endocytosis of both nanoparticles can be accomplished. The

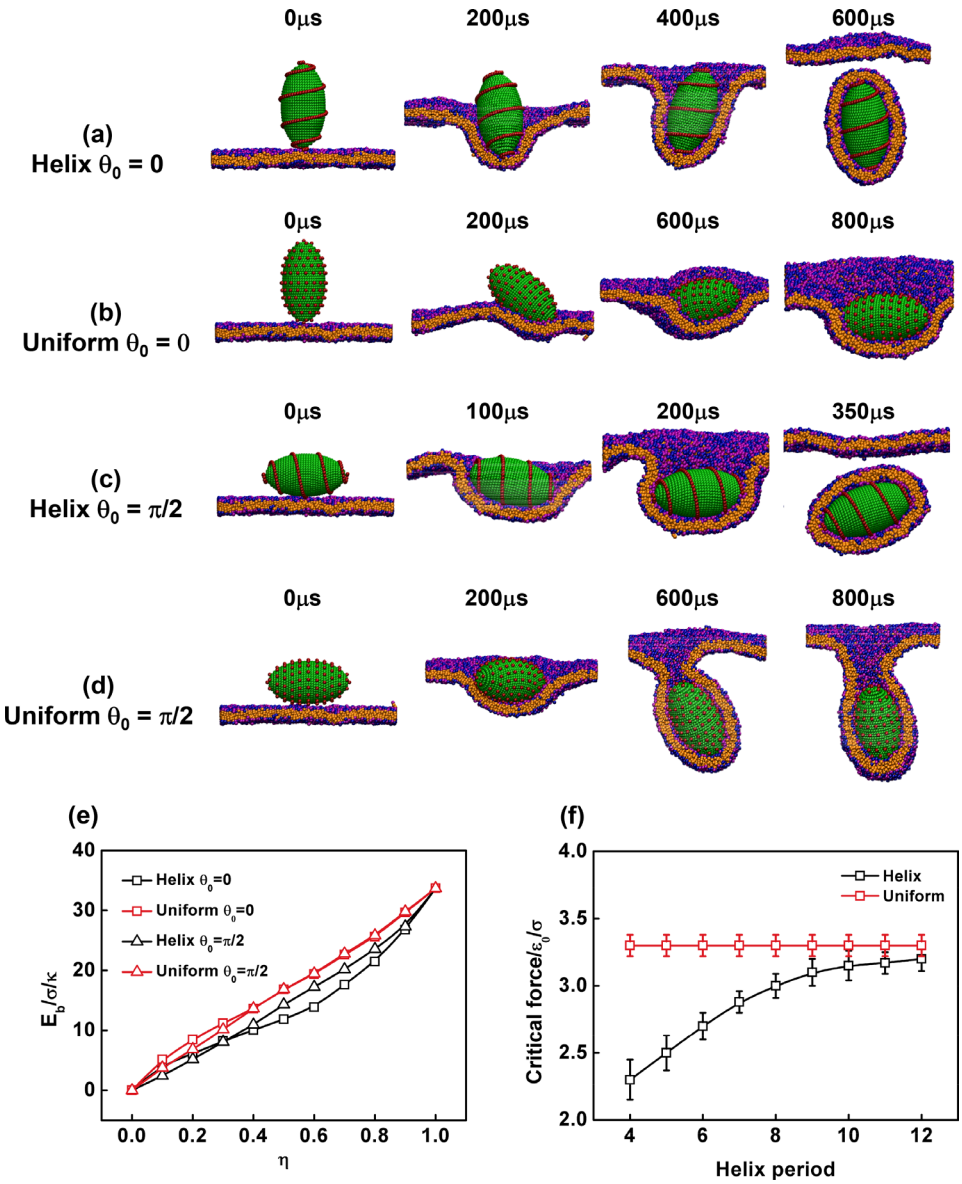

Figure 5. (a)–(d) Snapshots of the endocytosis process for nanoparticles with helical ligands (a), (c) and uniformly packed ligands (b), (d) under initial contact angles $\theta_0 = 0$ (a), (b) and $\theta_0 = \pi/2$ (c), (d). Ligand–receptor binding strength is set as $\varepsilon_{atr} = 3\varepsilon_0$. (e) Membrane bending energies during the endocytosis of those two nanoparticles with two initial contact angles, where $\varepsilon_{atr} = 4\varepsilon_0$. (f) Profiles of the critical force for the endocytosis of the two nanoparticles.

results are shown in Fig. 5(e), where the vertical and horizontal axes denote the membrane bending energy E_b/κ and the wrapping ratio (η) of the nanoparticle surface, respectively. The values of E_b/κ for all four cases start from $0\varepsilon_0/\kappa$ as $\eta = 0$ and increase to $33\varepsilon_0/\kappa$ when $\eta = 1$. However, the evolutions of these profiles are different from each other. Generally, the increased membrane bending energies of nanoparticle U are more intense than those of nanoparticle H. Therefore, the value of E_b/κ for nanoparticle U is higher than that for nanoparticle H until the end of endocytosis. This finding indicates that a lower energy barrier occurs before nanoparticle H completes its endocytosis than for nanoparticle U. Consequently, nanoparticle H has a greater endocytosis capability. According to the Helfrich formula and spinning endocytosis pathways of nanoparticle H, we can conclude that the enhanced endocytosis capability is a consequence of the smaller membrane curvatures (i.e. C_1 and C_2 in Eqn (9)). The spinning behaviour of the nanoparticle, especially the precession, can effectively reduce the membrane curvature during endocytosis.

For further comparison of the endocytosis capabilities between the two nanoparticles under the same ligand density ($\xi_L = 0.08/\sigma^2$), we calculated the critical force for endocytosis. When the receptor–ligand binding strength ε_{atr} is larger than the critical force, the nanoparticle can be completely endocytosed. The statistical results are presented in Fig. 5(f). Endocytosis cannot be accomplished when the period of the ligand helix is smaller than 4, which is mainly caused by the extremely inhomogeneous distribution of ligands when the helix period is equal to 1, 2 or 3 and is consistent with the reported theoretical investigations.[29] In this study, we provide the results only for cases with periods larger than 4 in Fig. 5(f). Nanoparticle U has a critical force of approximately $3.4\varepsilon_0/\sigma$, which means that when the receptor–ligand binding strength ε_{atr} is smaller than $3.4\varepsilon_0/\sigma$ the nanoparticle

cannot be completely endocytosed. However, for nanoparticle H, as the helix period of the ligands varied from 4 to 12, the critical forces increased from approximately $2.2\varepsilon_0/\sigma$ to $3.1\varepsilon_0/\sigma$, which is smaller than that of nanoparticle U. Obviously, an enhanced endocytosis capacity can be predicted for nanoparticle H. In addition, nanoparticle H has the smallest critical force when the helix period is 4. With an increase in the helix period, the critical force increases gradually and approaches the critical force of nanoparticle U ($3.4\varepsilon_0/\sigma$). Therefore, under a fixed surface ligand density, nanoparticles with smaller ligand helix periods can have a greater endocytosis capacity.

Effects of the initial contact angle of nanoparticles on the endocytosis pathway

When anisotropically shaped nanoparticles are internalized by membranes, the initial contact angles between nanoparticles and membranes can have an effect on the endocytosis behaviours.[25,50,51] In the present study, we performed simulations of nanoparticles that have different initial contact angles with the membrane and studied the results of endocytosis. In the simulations, the helix period of the ligands (denoted by P) decorated on nanoparticles was set to 5, and the initial contact angles (denoted by θ_0) varied from 0 (vertical contact) to $\pi/2$ (horizontal contact). Under each initial contact angle, the simulations were performed at least 10 times to make sure of the statistical accuracy.

The results are shown in Fig. 6. Figures 6(a)–6(c) present representative snapshots of nanoparticles with an initial contact angle $\theta_0 = \pi/6$, $\pi/3$ and $\pi/2$ during endocytosis. Figures 6(a) and 6(b) correspond to endocytosis initiated with an angle $\theta_0 = \pi/6$ and $\pi/3$, respectively. The figures show that the nanoparticle spontaneously 'stands up' and the major axis rotates perpendicular to the membrane. When the initial contact angle is increased to $\pi/2$, the nanoparticle is endocytosed with its major axis parallel to the membrane at all times. By carefully examining the endocytosis of nanoparticles with different initial contact angles, we found that the 'stand up' entry is observed only when the value of θ_0 is smaller than a critical value, which is approximately $4\pi/9$ (i.e. 'stand up' and 'laying down' entries can be observed under $0 \le \theta_0 \le 4\pi/9$ and $4\pi/9 < \theta_0 \le \pi/2$, respectively). In our 10-times statistics, all the nanoparticles exhibit precession behaviour when θ_0 is smaller than the critical angle. In Fig. 6(d), profiles of the θ angle with different initial contact angles during endocytosis are shown. From these profiles, we can directly observe the evolutionary orientations of the major axis. For the case $\theta_0 \le \pi/3$, θ angles are dramatically changed to a small value (approximately $\pi/12$) and fluctuate around this value during endocytosis. At $\theta_0 = \pi/2$, the θ angle is approximately $\pi/2$ at all times. Additionally, precession can be observed for the case $\theta_0 \le \pi/3$. The evolutionary φ angles during endocytosis under different initial contact angles are shown in Fig. 6(e). When $\theta_0 \le \pi/3$, the profiles of φ angles present sine/cosine waves before 300 μs. When $\theta_0 = \pi/2$, the φ angle is approximately 0. These results indicate that the nanoparticles decorated with helically distributed ligands have the capacity to spontaneously stand up and endocytose with precession even if they have a relatively large initial contact angle.

In most reported studies on the receptor-mediated endocytosis of non-spherical nanoparticles, the ligands are uniformly arranged. Generally, these nanoparticles will lie down rather than stand up before accomplishing endocytosis to obtain the maximum contact area with the membrane.[25,52] However, the present study shows that, for nanoparticles with helically decorated ligands, they have a tendency to spontaneously stand up (tip oriented) during the spinning stage and enter with precession.

Effect of the helix period of ligands on the endocytosis pathway

In addition to the initial contact angle, we studied the effects of the helix period (P) of ligands on the endocytosis of the studied nanoparticles because P is an important parameter of the helix. The number of ligand beads was kept constant at 147, and P varied from 4 to 10. All initial contact angles between the nanoparticles and membranes were set to $\theta_0 = 0$ (vertical contact) to guarantee endocytosis with spinning.

Figure 7 presents the endocytosis behaviours of nanoparticles with $P = 4$, 7 and 10. The snapshots during endocytosis are shown in Figs 7(a)–7(c), in which the major axes of the nanoparticles are denoted by arrows. All three types of nanoparticles are endocytosed with their major axes changing directions all the time. However, the transformation tendencies of the directions are different when the helix period varies. Before 100 μs, as P increases, the contact angles between the major axes of the nanoparticles and the membrane surface are closer to $\pi/2$ (perpendicular contact). After 100 μs the situation is reversed and, as P increases, the nanoparticles are more likely to lie down as shown in the snapshots, which indicates that the major axes are more parallel to the membrane. From Figs 7(d) and 7(e), we can clearly see the precession behaviours of the nanoparticle, and the evolutionary θ and φ angles during endocytosis are shown. Again, three stages can be observed during these procedures: spinning, spinning-free and end of endocytosis, which are denoted by the letters S, SF and E respectively in Fig. 7(e). The precession behaviours of nanoparticles with $P = 4$, 7 and 10 can be confirmed according to the sine/cosine waves during the spinning stage. However, the duration of these two stages varies under different P. With increasing P, the duration of the spinning stage is shortened and the spinning-free stage is lengthened. The solid and dashed lines in Fig. 7(d) indicate the maximum θ angle during the spinning stage and the average θ angle during the spinning-free stage. The results show that, with increasing P, the maximum θ angles during the spinning stage decreased but the average θ angles during the spinning-free stage increased.

This phenomenon indicates that, for a ligand helix with a smaller period, endocytosis exhibits a longer spinning stage. For larger P, nanoparticles show a shorter duration for the spinning stage but a longer duration of the spinning-free stage with larger contact angle. Therefore, the tendency for tip entry with precession behaviour can be effectively strengthened by reducing P. We can also predict the results when P approaches infinity ($P \to \infty$). In this case, the duration of the spinning stage will be 0 and of the spinning-free stage will be the duration of endocytosis. The contact angle will also be rather large. This endocytosis behaviour is very similar to the behaviour of nanoparticles with uniformly decorated ligands when attached to substrates (Supporting Information, Section S2). Actually, as P approaches infinity ($P \to \infty$), we can regard the ligands as being uniformly distributed on the surfaces of the nanoparticles.

Effect of the aspect ratio of nanoparticles on the endocytosis pathway

We examined the effects of the aspect ratio (denoted by λ) of the nanoparticle on the endocytosis behaviour. The semi-length of the long axis of the nanoparticle was fixed at $r_a = 15\sigma$, and the

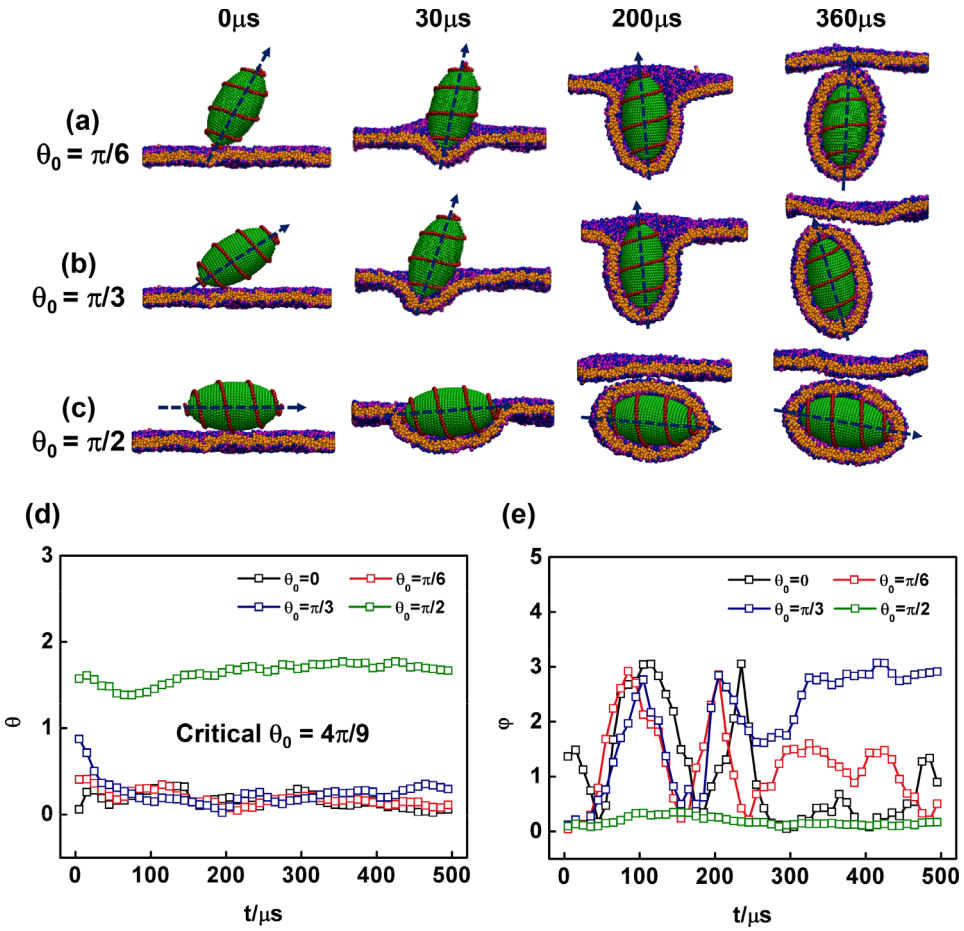

Figure 6. (a)–(c) Snapshots during endocytosis of nanoparticles with initial contact angles $\theta_0 = \pi/6$, $\pi/3$ and $\pi/2$. (c), (d) Profiles of θ and φ during endocytosis of nanoparticles with $\theta_0 = 0$, $\pi/6$, $\pi/3$ and $\pi/2$. Blue arrows in (a)–(c) denote the orientation of the major axis.

semi-length of the short axis r_b varied from 3 to 15σ. In this case, the value of λ changed from 0.2 to 1.0. Except for the aspect ratio, all other parameters were the same as the parameters from the previous section. All nanoparticles have the same mass, and 148 ligands are decorated on the surfaces. P is set to 4. The binding strength between the ligands and receptors was fixed at $4\varepsilon_0$. The initial contact angles between the nanoparticle and membrane varied from 0 to 2π.

The simulation results show that all these nanoparticles can be endocytosed under the applied conditions. The entire endocytosis process can be divided into the following three stages as discussed in the section 'Spin behaviour of nanoparticles with helically decorated ligands': spinning, spinning-free and end of endocytosis. At the first stage, the nanoparticle can spontaneously stand up and be endocytosed with precession. However, with changes in the aspect ratio of the nanoparticle, the critical initial contact angle for stand-up endocytosis with precession changes. The profile of the critical angle as a function of the aspect ratio is shown in Fig. 8. When the aspect ratio increases, the critical angle gradually increases. As the aspect ratio is increased to 1.0, the critical angle is increased to 2π. Therefore, a nanoparticle with a spherical shape can spontaneously stand up while being endocytosed under any initial contact angle. In addition to the critical angle, the duration of the first stage (i.e. spinning stage, denoted by $T_{spinning}$) is changed on varying the aspect ratio. Because the duration of the entire endocytosis process (denoted by $T_{endocytosis}$) also varies according to changes in the aspect ratio, we studied the values of $T_{spinning}/T_{endocytosis}$. The statistical results are shown in Fig. 8. This profile indicates that the value of $T_{spinning}/T_{endocytosis}$ is increased as the aspect ratio increases, which corresponds to an elongated spinning stage throughout the endocytosis process. These results indicate that a nanoparticle with a larger aspect ratio can more easily exhibit a 'gyroscope-like' endocytosis pathway. The spherical-shaped nanoparticle has the strongest capacity for precessional behaviour during endocytosis. On further increasing the aspect ratio to $\lambda > 1.0$, the simulation results indicate that the endocytosis pathways are similar to that of $\lambda \leq 1.0$. The spinning behaviour was also observed for $\lambda > 1.0$. For simplicity, those simulation results are not provided in the present work. In addition, we compared the cellular uptake capacities of two types of spherical nanoparticle ($\lambda = 1.0$). One nanoparticle has helically decorated ligands and the other has uniformly distributed ligands. The results are qualitatively identical to those for the oblate nanoparticles ($\lambda \neq 1.0$) in the present work. The helical distribution of ligands contributes to a stronger endocytosis capacity of nanoparticles under any aspect ratio.

DISCUSSION

The present theoretical simulations demonstrate a unique endocytosis pathway (precessional endocytosis) resulting from helically distributed ligands and reveals the mechanisms underlying this phenomenon. The rotation behaviour of nanoparticles during endocytosis has been predicted in theoretical work investigating

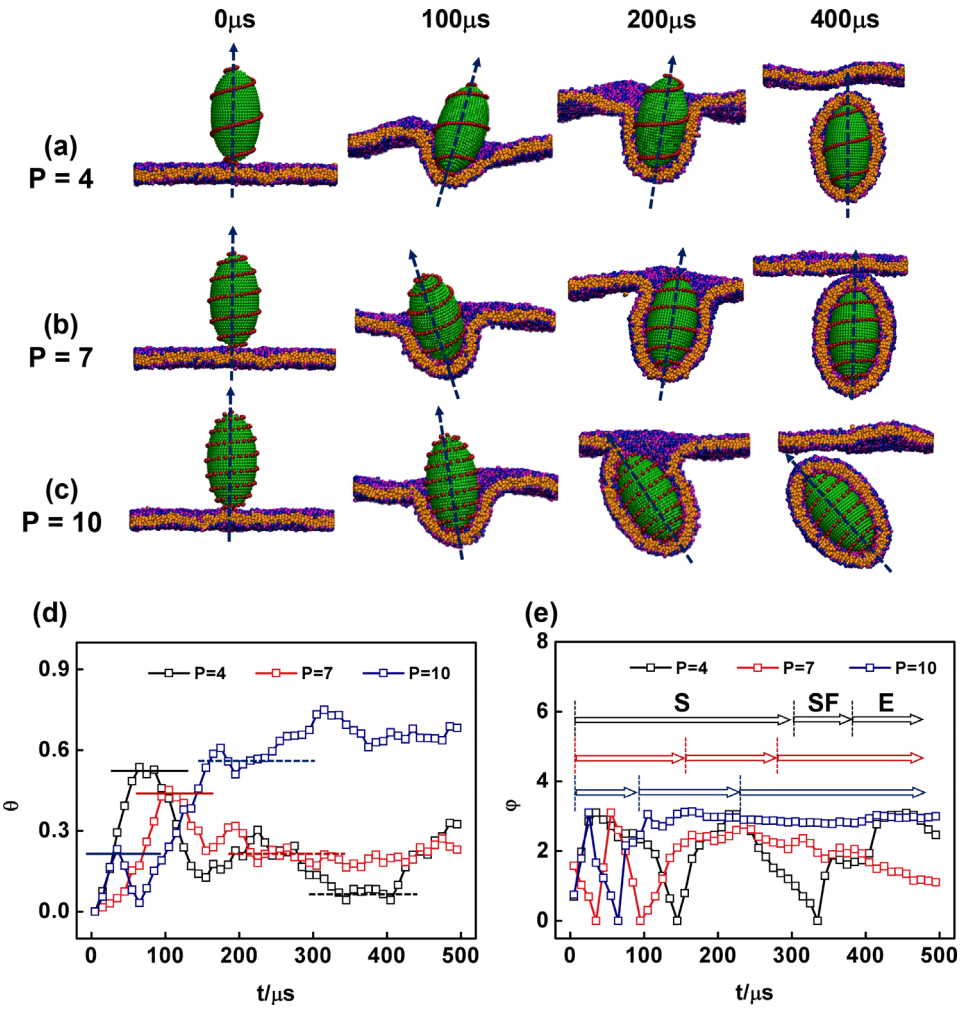

Figure 7. (a)–(c) Snapshots during the endocytosis of nanoparticles with a ligand helix period $P = 4$, 7 and 10. (d), (e) Profiles of θ and φ during the endocytosis of nanoparticles with different ligand helix periods. Solid and dashed lines in (d) denote the maximum θ during the spinning stage and average θ during the spinning-free stage, respectively. The spinning, spinning-free and end of endocytosis stages are illustrated in (e).

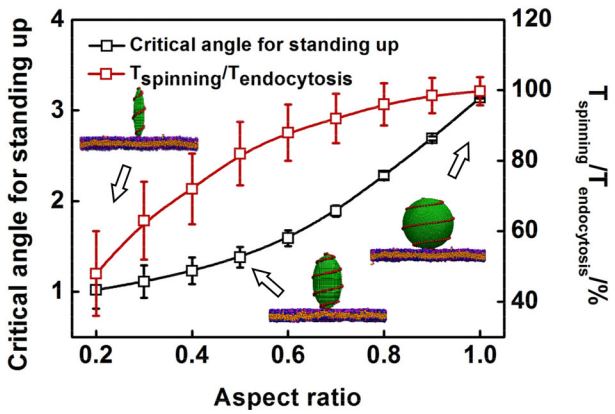

Figure 8. Critical angle for a spontaneous standing up endocytosis and the percentage of $T_{spinning}/T_{endocytosis}$ as a function of the aspect ratio (λ). Insets show the initial states of a system with nanoparticles at $\lambda = 0.2$, 0.5 and 1.0.

the cellular uptake of nanoparticles.[24,28,52] It is proved that these movements play important roles in endocytosis pathways. However, the rotation behaviour reported in existing work is almost a non-periodic two-dimensional movement. For example, an oblate-shaped nanoparticle enters the cell by changing its orientation within $\pi/2$ in the normal plane of the membrane.[53] In the present work, the unique precession behaviour is a periodic three-dimensional movement. The nanoparticle with helically decorated ligands rotates around the normal direction of the membrane for several periods, driven by the periodic torque acting on the nanoparticle. The present work reveals a novel rotation behaviour and could benefit further exploration for potential endocytosis pathways.

In addition to guiding theoretical investigations, the present work provides insights for understanding some experimental observations. For example, the results can serve as a clue for revealing the cellular internalization pathway of virus-like nanoparticles. In nature, a variety of virus particles have capsids with helical structures (e.g. Poxviridae). These natural nanoparticles are supposed to have unique cellular internalization pathways. Some evidence supports the different endocytosis behaviours of virus particles. For instance, Yoshida and colleagues investigated the exocytosis behaviours of fowlpox and pigeonpox (belonging to the family of Poxviridae),[54] and they found that these virus particles can exocytose in a tip-oriented manner, which provides a clue for the stand-up form of membrane penetration with spinning behaviour. However, because of the limitations of the experimental approach, the spinning behaviours could not be confirmed in their study.

In our simulations, the tip-oriented endocytosis process is reproduced, which is different from the side-oriented endocytosis of traditional nanoparticles. We found that these nanoparticles can spontaneously stand up when the initial particle–membrane contact angle (θ_0) is smaller than a critical value. Meanwhile this novel endocytosis behaviour cannot be observed when θ_0 is larger than this critical value. This prediction can be proved by some of the images provided in the work done by Yoshida and colleagues.[54] Additionally, our simulations suggest that these virus-like nanoparticles could endocytose with precession. This finding could serve as valid evidence for phenomena that have yet to be revealed experimentally. The precession behaviour revealed by our simulations may be an essential motivation for the substantial capacity to enter host cells shown by certain virus particles. Understanding this efficient internalization pathway is meaningful for enhancing the immunity of the human body and designing antibodies against these viruses.[55] Moreover, understanding the endocytosis pathways of these virus-like nanoparticles can provide theoretical insights for designing virus-mimetic drug delivery systems with improved cellular uptake performance. Compared with traditional nanoparticles or polymeric aggregates with smooth surfaces (i.e. uniformly packed ligands on the surface), novel particles with helical surfaces show enhanced cellular uptake capacity. Therefore, introducing helically arranged ligands on drug delivery system particles may represent an ideal approach for obtaining sufficient internalization performance and therapeutic efficacy.

It should be noted that the coarse-grained model adopted in the present work is an ideal system. The situation is much more complex for real *in vivo* or *in vitro* environments. For instance, the nanoparticles usually absorb proteins (e.g. serum proteins) before entering the cells, which could lead to a change of cellular uptake performance. Most of these proteins have stronger binding strength to the membrane receptor,[41] which could enhance the cellular internalization efficacy. Besides, as the absorbed proteins change the surface structures of the nanoparticles, we therefore predict that the precession behaviours discovered in the present work may not be observed in such a situation. In addition, the nanoparticles are assumed to be rigid body in our simulations, and maintain the original shape during the endocytosis. In reality, the nanoparticles could be soft (e.g. dendrimers, gel and polymer assemblies). When these soft nanoparticles are translocating through the membrane, the particle–membrane interaction pathways could be complicated,[25] due to deformation of the nanoparticles. In this case, spinning behaviours of nanoparticles may rarely occur. Another potential phenomenon that could happen for soft nanoparticles is the unpackaging of the carrier or endosomal escape. When designing a carrier system, the disassembly of the carriers during the entrance into the cells should be carefully considered. Fortunately, one can reduce or avoid these effects by several means. The key is to enhance the rigidity of the nanoparticles.[17] For a nanoparticle much more rigid than the membrane, deformation or unpackaging can be excluded. The results predicted in the present work could serve as a guidance for nano-carrier designing.

CONCLUSIONS

Using the CGMD simulation method, the endocytosis behaviour of a nanoparticle with helically decorated ligands was investigated. The endocytosis procedure for this nanoparticle can be divided into three stages: spinning, spinning-free and end of endocytosis. One of the most significant features of this endocytosis pathway that has not been observed in traditional pathways is precession in the initial stage (spinning stage). The lateral torque acting on the nanoparticle is responsible for the precession. This unique endocytosis pathway revealed in the simulations can be attributed to a reduced bending energy of the plasma membrane, which enhances the endocytosis capacity of the nanoparticles. The effects of the initial contact angle between the nanoparticles and membrane and the ligand helix period were examined. The results indicated that precessional endocytosis is favoured when the initial contact angle between the nanoparticle and the membrane is smaller than a certain value (i.e. a critical initial contact angle for precessional endocytosis). The precession behaviour can be effectively strengthened by reducing the ligand helix period or increasing the aspect ratio of the nanoparticle. The present study may provide useful information on cell internalization of virus particles with stripe-patterned surfaces and insights for the design of a drug delivery system with predominantly cellular uptake.

ACKNOWLEDGEMENT

This work was supported by the National Natural Science Foundation of China (51833003 and 51621002). Support from the Project of Shanghai Municipality (16520721900) is also appreciated.

SUPPORTING INFORMATION

Supporting information may be found in the online version of this article.

REFERENCES

1 Aoyama Y, Kanamori T, Nakai T, Sasaki T, Horiuchi S, Sando S *et al.*, *J Am Chem Soc* **125**:3455–3457 (2003).
2 Nagasaki Y, Yasugi K, Yamamoto Y, Harada A and Kataoka K, *Biomacromolecules* **2**:1067–1070 (2001).
3 Gao X, Cui Y, Levenson RM, Chung LWK and Nie S, *Nat Biotechnol* **22**:969–976 (2004).
4 Conner SD and Schmid SL, *Nature* **422**:37–44 (2003).
5 Marsh M and McMahon HT, *Science* **285**:215–220 (1999).
6 Mao J, Chen P, Liang J, Guo R and Yan LT, *ACS Nano* **10**:1493–1502 (2016).
7 Parton RG and Simons K, *Nat Rev Mol Cell Biol* **8**:185–194 (2007).
8 Liang J, Chen P, Dong B, Huang Z, Zhao K and Yan LT, *Biomacromolecules* **17**:1834–1844 (2016).
9 Jiang R, Jin Q, Li B, Ding D and Shi AC, *Macromolecules* **39**:5891–5896 (2006).
10 Yan LT and Yu X, *Macromolecules* **42**:6277–6283 (2009).
11 Byrne JD, Betancourt T and Brannon-Peppas L, *Adv Drug Delivery Rev* **60**:1615–1626 (2008).
12 Pippa N, Pispas S and Demetzos C, *Curr Pharm Des* **22**:2788–2795 (2016).
13 Jeong YI, Seo SJ, Park IK, Lee HC, Kang IC, Akaike T *et al.*, *Int J Pharm* **296**:151–161 (2005).
14 Lee H, Hu M, Reilly RM and Allen C, *Mol Pharm* **4**:769–781 (2007).
15 Nasongkla N, Shuai X, Ai H, Weinberg BD, Pink J, Boothman DA *et al.*, *Angew Chem Int Ed* **43**:6323–6327 (2004).
16 Sawant RR, Jhaveri AM, Koshkaryev A, Zhu L, Qureshi F and Torchilin VP, *Mol Pharm* **11**:375–381 (2014).
17 Sun J, Zhang L, Wang J, Feng Q, Liu D, Yin Q *et al.*, *Adv Mater* **27**:1402–1407 (2015).
18 Cho EC, Zhang Q and Xia Y, *Nat Nanotechnol* **6**:385–391 (2011).
19 Nativo P, Prior IA and Brust M, *ACS Nano* **2**:1639–1644 (2008).
20 Li Y, Kröger M and Liu WK, *Biomaterials* **35**:8467–8478 (2014).
21 Yue T and Zhang X, *ACS Nano* **6**:3196–3205 (2012).
22 Gao H, Shi W and Freund LB, *Proc Natl Acad Sci U S A* **102**:9469–9474 (2005).
23 Ding H and Ma Y, *Nanoscale* **4**:1116–1122 (2012).
24 Shi X, von dem Bussche A, Hurt RH, Kane AB and Gao H, *Nat Nanotechnol* **6**:714–719 (2011).

25 Guan Z, Wang L and Lin J, *Biomacromolecules* **18**:797–807 (2017).
26 Cooke IR and Deserno M, *J Chem Phys* **123**:224710 (2005).
27 Yuan H, Huang C, Li J, Lykotrafitis G and Zhang S, *Phys Rev E* **82**:011905 (2010).
28 Vácha R, Martinez-Veracoechea FJ and Frenkel D, *Nano Lett* **11**:5391–5395 (2011).
29 Schubertová V, Martinez-Veracoechea FJ and Vachá R, *Soft Matter* **11**:2726–2730 (2015).
30 Verma A, Uzun O, Hu Y, Hu Y, Han HS, Watson N *et al.*, *Nat Mater* **12**:588–595 (2008).
31 Li Y, Li X, Li Z and Gao H, *Nanoscale* **4**:3768–3775 (2012).
32 Xue J, Guan Z, Zhu X, Lin J, Cai C, Jin X *et al.*, *Biomater Sci* **6**:3251–3261 (2018).
33 Douglas T, *Science* **299**:1192–1193 (2003).
34 Lee ES, Kim D, Youn YS, Oh KT and Bae YH, *Angew Chem Int Ed* **47**:2418–2421 (2008).
35 Lim YB, Lee E, Yoon YR, Lee MS and Lee M, *Angew Chem Int Ed* **47**:4525–4528 (2008).
36 Xu Y, Ye J, Liu H, Cheng E, Yang Y, Wang W *et al.*, *Chem Commun* **1**:49–51 (2008).
37 Cai C, Li Y, Lin J, Wang L, Lin S, Wang XS *et al.*, *Angew Chem Int Ed* **52**:7732–7736 (2013).
38 Cai C, Lin J, Chen T, Wang XS and Lin S, *Chem Commun* **19**:2709–2711 (2009).
39 Cai C, Wang L and Lin J, *Chem Commun* **47**:11189–11203 (2011).
40 Cai C, Lin J, Lu Y, Zhang Q and Wang L, *Chem Soc Rev* **45**:5985–6012 (2016).
41 Walkey CD, Olsen JB, Guo H, Emili A and Chan WCW, *J Am Chem Soc* **134**:2139–2147 (2012).
42 Unsworth LD, Sheardown H and Brash JL, *Langmuir* **24**:1924–1929 (2008).
43 Xue J, Guan Z, Lin J, Cai C, Zhang W and Jiang X, *Small* **13**:1604214 (2017).
44 https://en.wikipedia.org/wiki/Parapoxvirus#/media/File:Parapox_Orf_virus_-_PHIL_5577_lores.jpg. Electron micro graph of parapoxvirus. [27 April 2019]
45 Berendsen HJC, Postma JPM, Gunsteren WFV, Dinola A and Haak JR, *J Chem Phys* **81**:3684–3690 (1984).
46 Schneider T and Stoll E, *Phys Rev B Condens Matter Mater Phys* **17**:1302–1322 (1978).
47 Bourov GK and Bhattacharya A, *J Chem Phys* **119**:9219–9225 (2003).
48 Grest GS, Lacasse MD, Kremer K and Gupta AM, *J Chem Phys* **105**:10583–10594 (1996).
49 Helfrich WZ, *Naturforscher* **28**:693–703 (1973).
50 Bahrami AH, *Soft Matter* **9**:8642–8646 (2013).
51 Dasgupta S, Auth T and Gompper G, *Nano Lett* **14**:687–693 (2014).
52 Li Y, Yue T, Yang K and Zhang X, *Biomaterials* **33**:4965–4973 (2012).
53 Huang C, Zhang Y, Yuan H, Gao H and Zhang S, *Nano Lett* **13**:4546–4550 (2013).
54 Hatano Y, Yoshida M, Uno F, Yoshida S, Osafune N, Ono K *et al.*, *J Electron Microsc (Tokyo)* **50**:113–124 (2001).
55 Mercer J, Schelhaas M and Helenius A, *Annu Rev Biochem* **79**:803–833 (2010).